# CALCULATIONS FOR SCENARIO A2 WITH THE SONAR PERFORMANCE MODEL MOCASSIN

J Ehrlich, Bundeswehr Technical Centre for Ships and Naval Weapons, Maritime Technology and Research, Research Branch for Underwater Acoustics and Marine Geophysics (FWG)
Berliner Straße 115, 24340 Eckernförde, Germany

## 1 INTRODUCTION

This paper presents the results of calculations with the sonar performance modelling tool MOCASSIN for the scenario A2 of the David Weston memorial workshop. The scenario describes a low-frequency active sonar application in shallow water in several test problems with varying parameters. This paper is organized as follows: The next chapter gives a short overview over the scenario and the test problems that were calculated. The full problem description can be found elsewhere in this proceedings[1]. Chapter 3 gives an introduction into the German Navy sonar performance modelling code MOCASSIN that was used for the calculations. The following chapter describes the points where the abilities of MOCASSIN and demands of the scenario did not meet fully and explains the choices taken for the calculations. Finally the selected results of the calculations are presented.

## 2 PROBLEM OVERVIEW

The scenario A2 describes the use of a low-frequency active sonar (LFAS) in shallow water with an omnidirectional source and a line array of receivers. The scenario consists of a basic problem, which is depicted schematically in figure 1, and several related problem with variations of the original setup and increasing complexity. The complete problem definition can be found in the article by Zampolli and Ainslie[1] in this proceedings. The short problem description in this chapter is for clarity only.

### 2.1 Basic problem

The basic problem, called A2.I, has a flat sand bottom with a bottom velocity $c_b$ = 1700 m/s, a density ratio between bottom and water of $\rho_b/\rho_w$ = 2 and an attenuation coefficient $\beta$ of 0.5 dB per wavelength. The attenuation in sea water is calculated according to the Thorp formula[3]. The bottom roughness could be described in two possible descriptions. Either by using a realization provided by the 2006 ONR reverberation modelling workshop or by using Lambert's law for the bottom scattering strength SS in the form of SS = $-27+10\log_{10}(\sin(\theta_{in})\cdot\sin(\theta_{out}))$ with $\theta_{in}$ being the incoming grazing angle, and $\theta_{out}$ being the outgoing grazing angle. The water has a constant sound speed of 1500 m/s and a constant density of 1000 kg/m$^3$.

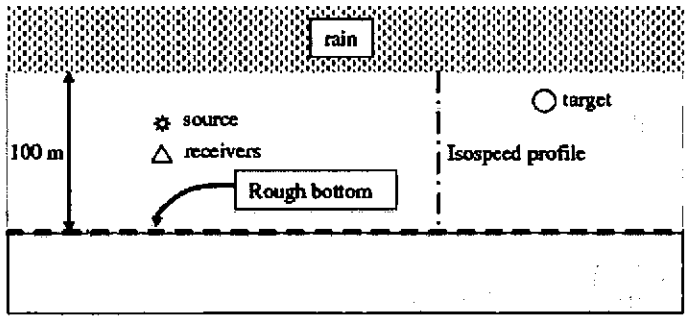


**Figure 1: Schematic drawing of the basic problem of scenario A2: LFAS sonar**

The source has an omnidirectional characteristic and is located at 30 m depth. The receiver is a horizontal line array with 65 equally spaced receivers in a line perpendicular to the drawing plane of figure 1. The element spacing is half a wavelength of the centre frequency of the transmitted pulse

and therefore varies with frequency. The array is located at 50 m water depth, with the centre hydrophone directly below the transmitter.

There are two different pulse types to be considered, a Gaussian pulse with 3 different centre frequencies of 250 Hz, 1 kHz and 3.5 kHz and linear frequency modulated pulse (LFM) from 1 kHz to 2 kHz. The Gaussian pulse is defined as

$$p(t) = A\cos(\omega_0 t)\, e^{-\frac{(t\Delta\omega)^2}{2}} \quad \text{with } \omega_0 = 2\pi f_0 \text{ and } \Delta\omega = \pi \frac{BW_{3dB}}{\sqrt{\ln(2)}} \qquad (1)$$

$BW_{3dB}$ is the bandwidth between the -3 dB points which are at $\pm f_0/20$ around the centre frequency $f_0$. The pulse has to be cut off the the time $T_H/2$ after the maximum when the envelope of the pressure has dropped to –100 dB re 1 μPa$^2$ . The value for the amplitude $A$ is chosen to give the energy source level $SL_E$ of 200 dB re 1 μPa$^2$s at 1m in all cases. The energy source level is defined as

$$SL_E = 10\log_{10} \int (p_{1m}(t))^2 dt \qquad (2)$$

with $p_{1m}$ being the pressure at 1 m distance from the source.

The LFM pulse with a duration of 2s starts at 1 kHz and goes up to 2 kHz and is given as

$$p(t) = A\sin\left(2\pi\left(a(t-t_0) + k/2(t^2 - t_0^2)\right)\right), \quad \text{with } a = f(t_0) + k\, t_H/2 \qquad (3)$$

Again, the value of the amplitude $A$ was chosen accordingly to produce an energy source level of 200 dB re 1 μPa$^2$s at 1 m distance.

| | Duration $T_H$ [sec] | Amplitude $A$ [kPa] |
|---|---|---|
| Gaussian 250 Hz | 0.2 | 73 |
| Gaussian 1 kHz | 0.05 | 146 |
| Gaussian 3.5 kHz | 0.0014 | 273 |
| LFM | 2 | 10 |

**Table 1: Parameters for the four source pulses of the problem specification**

The target is a sphere with radius 7m which has a target strength of close to +8 dB. It is located at a depth of 10 m.

The noise consists of rain noise according to the rain spectrum from the APL-UW model[3] (equation 60), with a rainfall rate of 1 mm/h. This model describes the noise via a uniform distribution of surface dipoles. Rain noise should be disregarded for the 250 Hz case.

## 2.2 Quantities of interest

The participants were asked to provide results of calculations of the following quantities, both before signal processing (marked with A) and after signal processing (marked with B):

A.1: Noise spectral density level, NLS, at the receiver

A.2: Echo sound-pressure level, EL(r)

A.3: Reverberation, RL(r), sound-pressure level of reverberation at the receiver

A.4: Signal to reverberation ratio: SRR*(r)* = EL*(r)* – RL*(r)*.

A.5: Propagation loss PL at the target locations and at 99m depth

B.1: Beamformer output: $EL_{bf}(r)$

B.2: Reverberation after beamforming $RL_{bf}(r)$, beamformer output for reverberation only.

B.3: Noise spectral density level $NLS_{bf}$, after beamforming, defined

B.4: Signal to reverberation ratio after beamforming: $SRR_{bf}(r) = EL_{bf}(r) - RL_{bf}(r)$ .

B.5: Echo Level after the Matched Filter: $EL_{mf}(r)$

B.6: Reverberation Level after the Matched Filter:$RL_{mf}(r)$

B.7: Noise level, $NL_{mf}$ after matched filtering

B.8: Signal to background (noise+reverberation) ratio $SNR = EL_{mf}(r) - 10\log_{10}\left(10^{RL_{mf}/10} + 10^{NL_{mf}/10}\right)$

## 2.3 Other problems

Building on the basic problem other problems were defined that increase the complexity in several aspects. The exact problem definition for all subsequent problems A2.II – A2.VIII can be found in reference[1] in this proceedings. Here only a short overview is given over the problems for which solutions are presented.

**A2.II = Baseline Problem A2.I + 10 m/s wind speed**

Problem A2.II has the same parameters as the basic problem A2.I but the surface has a roughness that corresponds to a fully developed sea at a wind speed of $w$ = 10 m/s.

**A2.III = Problem A2.I + cutoff duct and winter profile**

Problem A2.III introduces non-constant sound speed profiles into the scenario. It consists of two subcases A2.III1 with a constant gradient "winter" profile and a cut-off duct "summer" profile. The other parameters are identical with the basic problem (i.e. rain, no wind).

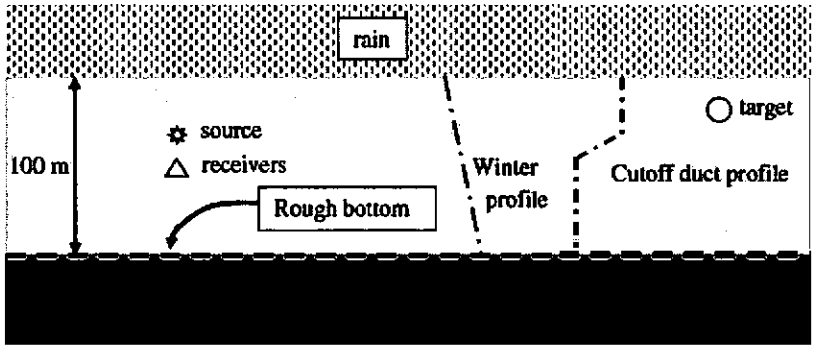


**Figure 2: Schematic drawing of problem A2.III with winter profile and summer profile (cut-off duct)**

# 3 THE SONAR PERFORMANCE MODEL MOCASSIN

## 3.1 History of the model

For the calculations the German Navy's sonar performance model MOCASSIN was used. The acronym MOCASSIN stands for Monte Carlo Schall-Strahlen Intensitäten, which can be translated as Monte Carlo Sound Ray Intensities. Strictly speaking MOCASSIN is the name of the simulation programme suite in use by the Navy, complete with graphical user interface and data bases for world-wide environmental parameters and sonar/target data. The underlying propagation model, which was used for the scenario calculation and is described here briefly is called SIPSI (Single profile stochastic intensities). But it has become usual to call it MOCASSIN as well in publications and it will be done so here as well.

The model has been developed at the former Federal Armed Forces Research Institute for Underwater Acoustics and Marine Geophysics (FWG) for active sonars in shallow waters with highly variable sound speed conditions and poor knowledge on the input data. The variability is of stochastic nature. It may be sufficiently strong to influence the average sound pressure level and cause deviations from the values of sound pressure level expected with a non-variable sound speed structure.

Moreover, in most shallow water areas the water depth and bottom reflectivity vary considerably over ranges of interest, so that the model has to account for range dependent water depths as well. Given these requirements the most suitable numerical scheme seemed to be raytracing. The only constraint arising from this is a limitation to sufficiently high acoustic frequencies and sufficiently large water depths.

The origins of this programme date back to the late 1970s where Schneider published the idea and first results[4,5]. Additional background material can be found in an article by Sellschopp[6]. Over the years there have been several publications of comparisons between calculations and experimental data[7-10] but only few comparisons to other models[11].

## 3.2 Stochastic raytracing

The main feature that sets MOCASSIN apart from other propagation models is the stochastic raytracing approach. This method uses a Monte Carlo approach for the stochastic change of ray directions and was found to be a very effective way of accommodating the acoustic forward scattering which is caused by variations of the sound speed in the water column. In line with the incoherent transmission loss data from the experiments, with the model's stochastic approach and with operational conditions and needs, the model calculates incoherent TL only and requires only one sound speed profile to be specified.

The propagation of underwater sound is computed in the optical or geometric acoustic approximation of the wave equation, better known as raytracing. This implies that the acoustic wave length $\lambda$ is small compared to any other structure length $L$ of importance for the propagation $\lambda << L$. The most dominating structure length is evidently the water depth $H$, thus it is required that $\lambda << H$. This poses no real restrictions for active ASW-sonar's since the lowest frequencies used are in the low kHz region with wave lengths smaller than about 1 m allowing for water depths as shallow as 30 m. In case of a depth dependent sound speed layering $C(z)$ the condition to be met is:

$$\frac{\lambda}{C}\left|\frac{dC(z)}{dz}\right| << 1 \qquad (4)$$

which means the sound speed variation should be small over a wavelength.

The vertical sound speed profile $C(z)$ will be approximated by linear segments, so that horizontal layers of constant sound speed gradients are formed. This allows for very effective numerical raytracing equations in which the ray paths are either straight lines ($dC/dz = 0$) or arcs of a circle ($dC/dz \neq 0$). The calculation domain is divided into rectangles. The corners of the rectangles are defined in z by the points where the linear sound speed segment start and end and in range by the points where linear segments of the bathymetry start and end. For large parts with constant

bathymetry a partition in range is chosen in a way that the aspect ratio of the calculation rectangles are not too large.

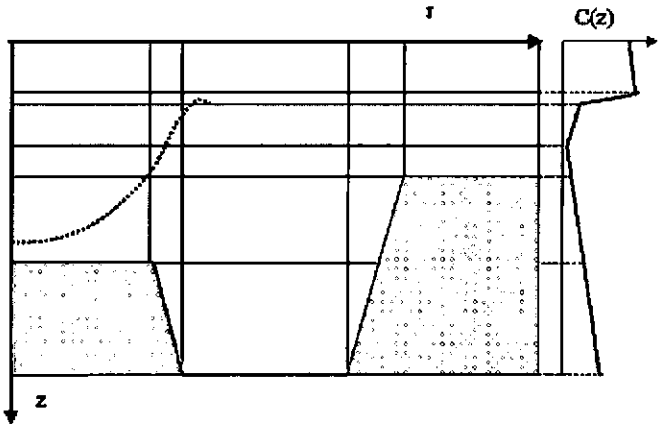


**Figure 3: Schematic drawing of the calculation boxes from MOCASSIN defined by the bathymetry and the linearized sound speed profile (right). The blue dotted line on the left shows a resulting ray.**

The input sound speed profile should be sufficiently sampled, that the fine structure important for the highest frequency considered is included. However, a locally measured vertical fine structure is only effective, if it is persistent over a sufficiently large horizontal distance, otherwise the propagation can erroneously be dominated by a local feature. If necessary, a linearization process reduces the number of points to an appropriate value for further calculations.

In some ocean areas as the Baltic-Sea or Skagerrak the sound speed stratification is highly variable with range, over distances which are short relative to the propagation distance, which leads to horizontal sound speed gradients, e.g. the thermocline may frequently change depth, while the main features of the vertical sound speed profiles are conserved.

In these and similar cases the horizontal sound speed variability may often be described stochastically i.e. the variation may be assumed to occur at random. The acoustic effect is, that additional losses (leakage) from sound channels occur or vice versa acoustic energy may be trapped in sound channels. To model this effect, a diffusion approximation is assumed in which the diffusion constant $D$ has been made dependent on the sound speed profile $C(z)$

$$D(z) = D_0\left(1 + g_0\left|\frac{dC(z)}{dz}\right|\right)^2 \qquad (5)$$

$D_0$ is an empirical input quantity in the range of $10^{-10} \le D_0 \le 10^{-6}$ and $g_0$ is a scale factor with numerical value one second. This assumes, that the angular deviation $\Delta\phi$ of the rays propagation angle from the deterministic conditions at the end of the layer is given by a Gaussian probability density for $\Delta\phi$ with

$$\overline{\Delta\phi} = 0 \quad , \qquad \sigma^2 = \overline{\Delta\phi^2} = 2\,DS;$$

where $S$ is the path length in that layer. The angular change is actually not applied at each layer boundary, but is accumulated over several layers $i$ for a path length $S_{sum}$

$$S_{sum} = \sum S_i \qquad \text{and} \quad \sigma^2 = \sum S_i\, D_i(z) \qquad (6)$$

and is applied in the range interval $DX_{STC} \le S_{sum} \le 2\,DX_{STC}$. This provides a certain randomizing of the locations where the angular changes are applied. For statistical meaningful results many events should occur over the total propagation range ($DX_{STC} << max.range$) and for the diffusion approximation to hold, the angular change should be small (i.e. $\sigma^2 = 2\,D\,S << 1$ ). On the other hand for computational efficiency $DX_{STC}$ should be large. The empirical compromise for the value $DX_{STC}$ in meter is used for is

$$DX_{STC} = \max\left(1000, \min(200\sqrt[3]{d_w}, max.range/20)\right) \quad (7)$$

where the dimensionless number $d_w$ is the value of the water depth in meter. In depths larger than 1500 m the sound speed structure is assumed to be invariant and no stochastic angular changes of the propagation angle are applied, i.e. $D$ ($z \geq 1500$ m) = 0.

Numerical values for the diffusion constant $D_0$ have been determined empirically by modelling various environments. The following quantities are recommended:

$$D_0 \begin{cases} \leq 10^{-9} & \text{quasi deterministic (no variability )} \\ = 10^{-8} & \text{low variability ( North Sea and most areas )} \\ = 10^{-7} & \text{high variability ( Baltic, Skagerrak )} \end{cases}$$

## 3.3 Propagation loss computation

In contrast to deep water raytracing models, which compute the intensity at one point in depth and range by ray divergence methods, this model accumulates the intensity of rays penetrating receiver window of vertical size $\Delta$, at depth $z$ and range $r$. A maximum of 100 sample points in range is allowed and a maximum of 30 consecutive vertical receiver windows, spanning the depth range from $z_0$ to $z_{max}$ = $z_0 + n\,\Delta$, with $1 \leq n \leq 30$.

Note that the loss is an incoherent average over the depth interval $\Delta$ and too small values of $\Delta$, will result in rapidly fluctuating loss curves because of insufficient ray statistics in the receiver window, as this is no eigenray solution. In order to give meaningful results a large number of rays has to be used, usually in the order of several thousands. Thanks to the easy ray calculation process with stepwise linear sound speed profiles the overall calculation is still very quick.

The standard vertical source characteristic is modelled by a parabola. The energy radiated decreases with angle $\phi$ as:

$$E(\phi) = 1 - 2\left(\frac{\phi - \phi_i}{\phi_0}\right)^2, \qquad |\phi - \phi_i| \leq \frac{\phi_0}{\sqrt{2}} \quad (8)$$

where $\phi_i$ is the tilt angle against the horizontal and $\phi_0$ is the opening angle between the two 3 dB points. A single ray represents the intensity in the angular interval $\Delta\phi = \sqrt{2}\phi_0 / N$ which is sufficiently approximated by $I(\phi) = E(\phi) \cdot \Delta\phi$ if the number of rays $N$ in the above interval is sufficiently large. The numerical realisation assumes a constant intensity for all rays and attributes larger angular intervals to a single ray according to this energy distribution.

The use of such an approximated beam profile is allowed for long range propagation with fairly realistic sonar beams in shallow water where the farfield intensity is dominated by rays with small inclinations. Rays with steeper angles are not considered because they quickly loose energy by numerous reflections on the seafloor and the surface. In order to use the model for other scenarios as well several other beampattern have been added, including sidelobes. Therefore it is now possible to calculate especially the reverberation for short distances which is dominated by the scattering from energy from the sidelobes. Figure 4 shows a schematic representation of an unshaded rectangular beampattern with sidelobes. A completely omnidirectional beampattern, as specified in the scenario, can not be chosen but a clipped omnidirectional pattern with 90 degress beamwidth is sensible approximation for the desired farfield calculations. The rays with steeper angles will decay relatively soon and not contribute to the farfield results.

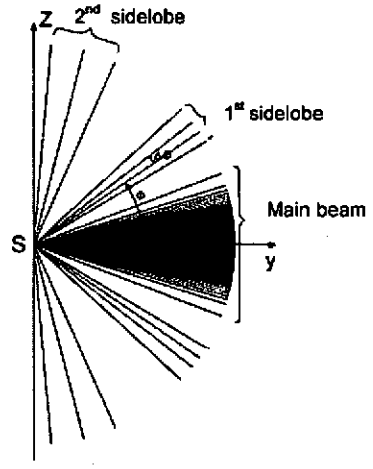


**Figure 4: Idealized beampattern in MOCASSIN with sidelobes**

This type of ray-tracing approach in which the intensity between two adjacent rays is not interpolated in space, is mathematically only exact in the limit of an infinite number of rays. However, for most practical applications a few thousand rays will constitute a sufficient approximation. Deviations in the computed loss occur, if different numbers of rays or different sequences of random numbers are used. These deviations are generally insignificant at high intensity regions and will be noticed mainly at large intensity gradients or in low intensity (high loss) areas into which the intensity has been carried by only a few rays. Smoothing the propagation loss curves by splines will reduce these differences.

## 3.4 Boundary conditions

In order to describe the propagation of sound energy and the interaction of sound with the sea properly, several aspects have to be considered. For that purpose MOCASSIN includes several models describing the interaction with the boundaries seafloor and surface.

**Medium absorption**

The formula developed by Francois and Garrison[12] is used to compute the sound attenuation due to the medium. This formula is applicable in North Sea and North Atlantic as well as in low salinity water of Fjords and the Baltic Sea, where the Thorp formula fails. Input parameters are salinity, temperature and acidity (pH-value).

**Seafloor interaction**

The bottom topography is modelled by linear range segments for the propagation range considered. Each bottom segment may be characterized by a different bottom reflectivity, depending on the bottom type. Several bottom type classification schemes are available. The reflectivity values for each bottom type have been calculated in advance using the numerical simulation tool OASES[13] with the bottom sound speed profiles provided by Hamilton[14] for given grazing angles and frequencies. These tabulated values are then interpolated for the actual frequency and grazing angle that is needed in a MOCASSIN calculation.

The bottom reverberation is computed from the backscattering strength $BS$ of a modified Lambert's law, where $\phi$ denotes the rays grazing angle with the bottom interface.

$$BS = 10\log_{10}(\mu) + n \cdot 10\log_{10}(\sin\phi) \tag{9}$$

The values for the Lambert constant $\mu$ and the exponent $n$ of the angular term depend on the bottom type. With the parameters $10\log_{10}(\mu) = 27$ and $n = 2$ the standard Lambert's law is recovered, as it was specified in the scenario definition.

**Sea surface interaction**

The sea surface is considered to be stochastically rough. An acoustic plane wave impinging on this surface will partially be reflected specularly and partially be scattered into other directions. The total energy density $\gamma$ of the reflected and the scattered field $\gamma_s$ can be written as:

$$\gamma(\phi,\phi_0,H_{1/3},f) = \delta(\phi-\phi_0)e^{-g} + (1-e^{-g})\gamma_S(\phi,\phi_0,H_{1/3},f) \tag{10}$$

with $\phi_0$ being the incident grazing angle, $\phi$ the outgoing grazing angle, $\delta$ the delta function and $g$ the Rayleigh parameter which determines the partitioning of scattered and reflected energy

$$\sqrt{g} = 4\pi\frac{\sigma}{\lambda}\sin(\phi_0) \tag{11}$$

where $\sigma$ denotes the rms wave height. The significant height of the windsea $H_{1/3} = 4\ \sigma$ is an input parameter, while the slope is determined from the correlation length of the windsea in shallow water derived from own measurements of FWG in the North Sea and the Baltic[15].

The above angular energy density $\gamma$ is utilized in the raytracing as probability density; the ray impinging on the rough sea surface with angle $\phi_0$ will propagate onwards with angle $\phi$ according to the

probability density $\gamma$. Thus with a sufficiently high number of surface contacts the angular density is modelled, however not at one point in range but distributed over the entire propagation distance

The influence of a bubble layer below the surface is modelled with a modification of the semi-empirical model by Christian[16]. The parameters were fitted to match the results of own measurements by FWG from a platform in the North Sea.

The reverberation from the sea surface is computed from the empirical backscattering strength formula developed by Chapman and Harris[17].

# 4 CALCULATIONS

The MOCASSIN code has several limitations with regard to some specifications of the scenario A2 This makes it impossible to calculate every quantity exactly as it was specified in the scenario definition. In order to be able to compare the MOCASSIN results with other codes some simplifying assumption had to be taken.

**1. Bistatic calculations**

The scenario A2 demands bistatic calculations, because the source and the receiver are not co-located. At the present time MOCASSIN only allows monostatic calculations. Therefore the setup for the calculations has been changed. The receiver was moved to the position of the source at the depth of 30 m. Apart from very small ranges the difference in range and grazing angle between the original bistatic configuration and the monostatic approximation is negligible, with the exception of problem A2.IV with upslope bathymetry. In this case it is important if the receiver is located at the water depth of the shallower part or below. Some discrepancies between bistatic and monostatic calculations might be expected in problems with the summer profile as well.

**2. Pulse forms and pulse length**

Strictly, the echo level is defined as 10 times the logarithm of the maximum of the sound pressure squared received during a certain observation time. This definition automatically includes the effects of the pulse form, frequency content and pulse length of the signal. As a traditional raytracing code MOCASSIN does not include these effects directly but calculates narrowband values for a given frequency, usually for the centre frequency of the signal. This is also true for the input value source level. The assumed energy source level $SL_E$ of 200 dB re 1 µPa$^2$s according to equation 1 takes the energy of the pulse into account. The translation into a frequency domain picture with the approximation by a monofrequent signal gives an equivalent source $SL_{eq}$

$$SL_{eq} = 10\log_{10}\left(\frac{A^2}{2}\right) \tag{12}$$

as the logarithm of the rms value of the amplitude $A/\sqrt{2}$. For real broadband signals like the LFM pulse from this scenario that might be a poor approximation. Similarly the noise level is frequency dependent but this is included by averaging over the frequency band of the receiver.

**3. Beamfoming and matched filtering**

In scenario A2 a sonar with a linear array of receivers and matched filter signal processing is assumed. The calculation of the quantities beamforming gain or matched filtering gain is not in the scope MOCASSIN. Therefore, both signal processing steps are not directly modelled in MOCASSIN. But there are indirect ways to get approximations for the signal processing gain. But the reader has to be cautioned that the methods explained below are not rigorously tested and the accuracy may be limited.

For the beamforming gain the approximate formulas for the directivity index $DI_N$ against noise and $DI_R$ against reverberation are used as an approximation

$$DI_N \approx 21 - 10\log_{10}(\vartheta_{3dB}) \quad \text{and} \quad DI_R \approx 10\log_{10}(360°/\vartheta_{3dB}) \cdot$$
$$DI_N = 10\log_{10}\left(\frac{2L}{\lambda}\right) \quad \text{and} \quad DI_R \approx 10\log_{10}(360°/\vartheta_{3dB}) \cdot \qquad (13)$$

Both values are in decibels with $\vartheta_{3dB}$ being half the horizontal beam width, defined by the 3 dB points where the sound intensity has dropped off to half the maximum value.

For the problem of the matched filter gain another assumption can be made. MOCASSIN contains formulas for the detection threshold for two types of signal detection, the pure energy detection without any knowledge of the signal and the detection of completely known signals. It is assumed that the beamformed signal before the matched filtering corresponds to energy detection, whereas matched filtering gives the maximum value for signals with known signal structure. Therefore the processing gain from matched filtering can be estimated by the difference between the detection thresholds for the two types of detection, both against noise and against reverberation. The detection thresholds $DT_N$ against noise are taken from Urick[18] and $DT_R$ against reverberation from Kroenert[19] as

$$DT_N^{coher} = 10\log_{10}\left(\frac{d}{2T}\right) \qquad DT_R^{coher} = 10\log_{10}\left(\frac{d}{2B}\right)$$
$$DT_N^{incoh} = 5\log_{10}\left(\frac{d \cdot B}{T}\right) \qquad DT_R^{incoh} = 5\log_{10}\left(\frac{d \cdot T}{B}\right) \qquad (11)$$

where $d$ stands for the detection index, $B$ the (effective) bandwidth and $T$ the (effective) time duration of the signal. The superscript *coher* marks the values for the matched filter signals (coherent detection) and *incoher* the incoherent energy detection.

Taking the definitions for effective bandwidth and effective pulse duration of Burdic[20] for the signals with Gaussian envelope

$$B = \frac{\Delta\omega}{\sqrt{2\pi}} \quad \text{and} \quad T = \frac{\sqrt{2\pi}}{\Delta\omega} \qquad (12)$$

the above equations actually give a negative processing gain of –3 dB, assuming a realistic detection index of $d$ = 16, both for noise and reverberation. The theoretical maximum gain, which is given by the value $B \cdot T$ gives exactly unity. This shows that the Gaussian signals are not well suited for matched filter processing. In the calculations for scenario A2 a processing gain of 0 dB has been assumed, that means there is no difference between the beamformed and the match filtered echo levels (categories B1 and B5). The much longer LFM signal, on the other hand, is much better suited for matched filtering and the equations 11 give a processing gain of $DT^{incoh} - DT^{coher}$ = 13.5 dB both against noise and reverberation.

Both for the beamforming and the matched filtering the gain is attributed only to the noise and reverberation terms as decrease and not to the echo signal as an increase. This is somewhat arbitrary but without further knowledge of the processing in the sonar an assumption has to be made. However the signal-to-reverberation or signal-to-noise ratios are the same regardless how you distribute the gain. Therefore theses values can be compared with the results from other codes that consider the signal processing in a different way.

# 5 RESULTS

In this chapter the results of the MOCASSIN calculation for selected results from the test problems are presented. Due to the number of test cases, signals and quantities not all results can be shown.

## 5.1 Results for the basic problem A2.I

First the results for the basic isovelocity problem A2.I with the Gaussian signal at 1000 Hz centre frequency are shown. Apart from the system independent quantities that were asked for in the problem definition the sonar performance modelling tool MOCASSIN also produces results that incorporate the detection process. As an example the right picture of figure 6 shows the probability of detection for that case. Up to 30 km the probability of detection is nearly 100 % independent of depth, except for the top layer where an additional absorption term accounts for losses in the forward scattering due to surface roughness.

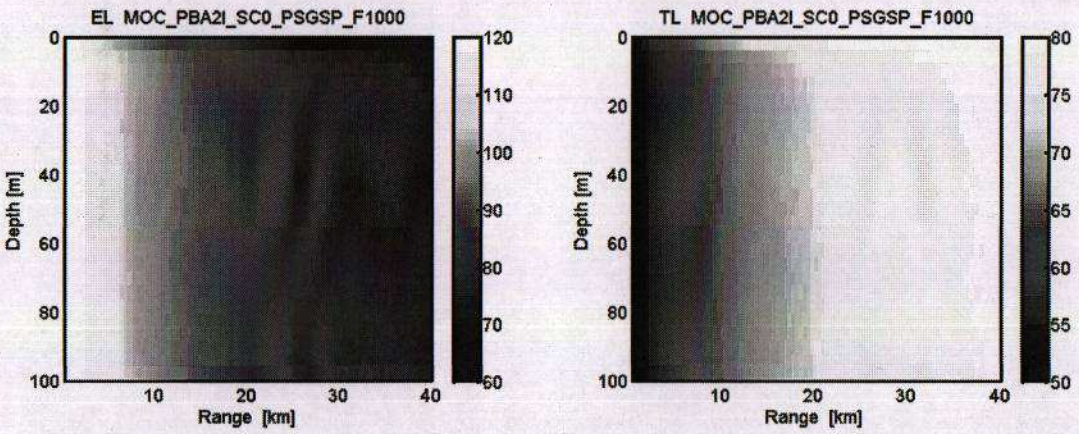


Figure 5: Echo level in dB re 1 μPa2 (left) and transmission loss in dB re 1m2 (right) for problem A2.I with Gaussian signal (1kHz).

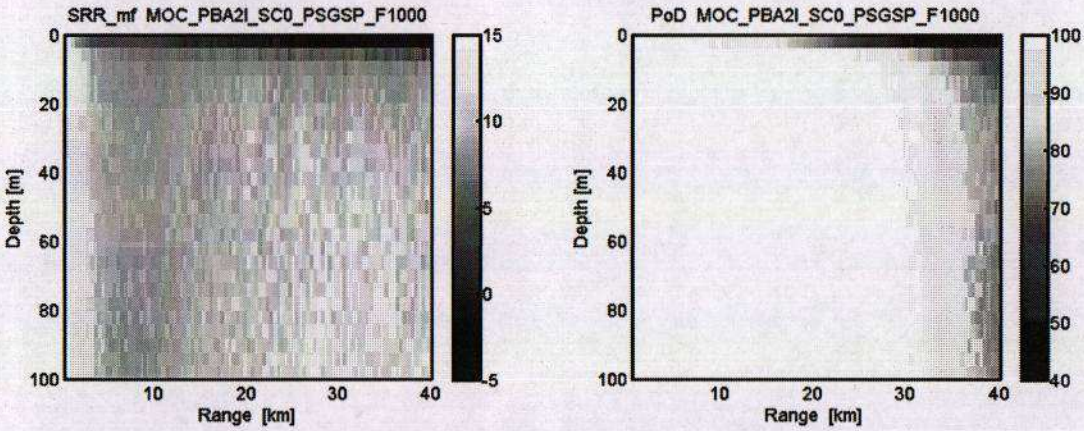


Figure 6: Signal-to-Reverberation Ratio after beamforming in dB and matched filtering (left) and probability of detection in percent (right) for problem A2.I with Gaussian signal (1kHz).

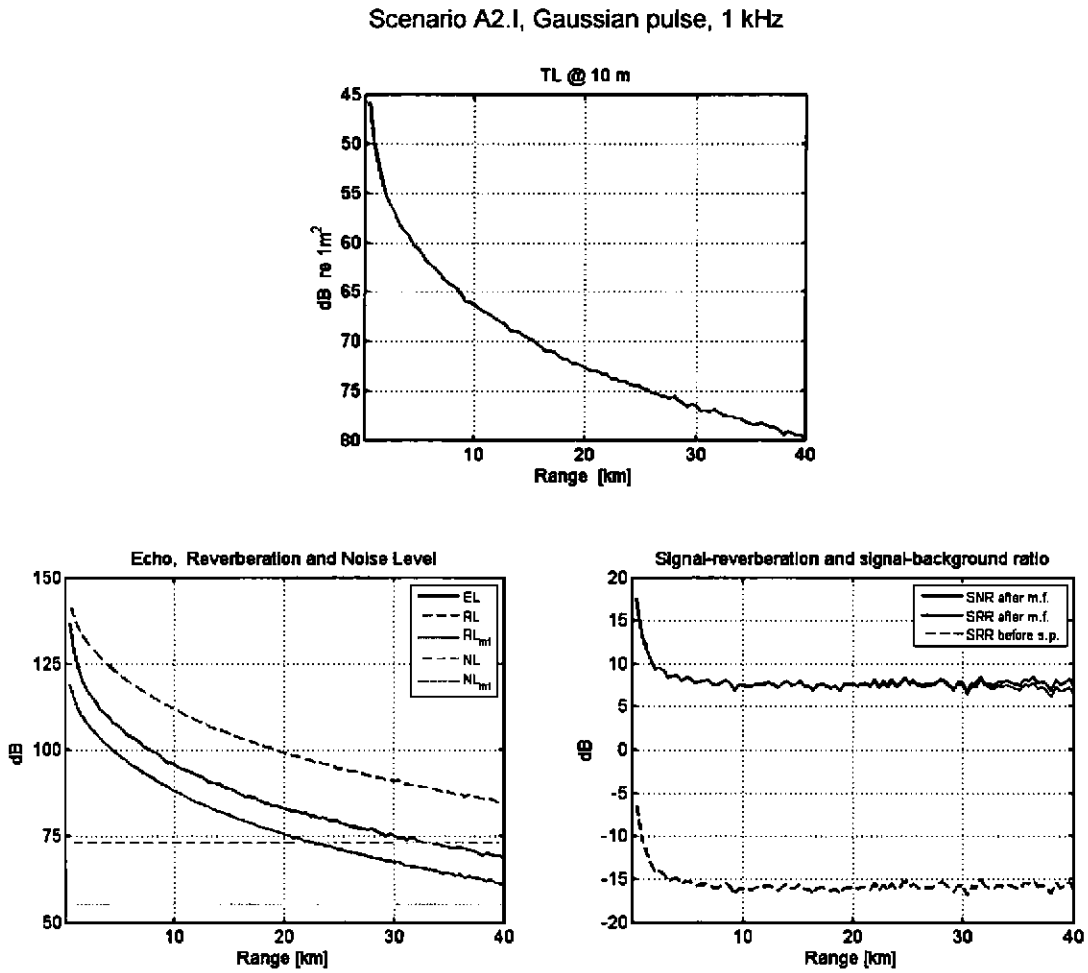


**Figure 7: Required quantities for scenario A2.I with Gaussian signal, 1 kHz centre frequency:**

**Top: Transmission loss at target depth (A5),**

**Left: Echo level EL (A2, B1, B5) identical before and after signal processing (s.p.)**
**Reverberation level before s.p. RL (A3), and after s.p. RLmf (B2, B6)**
**Noise level before s.p. NL (A1) and after s.p. NLmf (B3, B7)**

**Right: Signal to reverberation before s.p. SRR (A4) and after s.p. SRRmf (B4)**
**Signal to background SNR (noise+reverberation) after s.p. (B8)**

Figure 7 shows plots of the required quantities A1 - B8 from the scenario definition versus range. For the Gaussian signals the values after beamforming and matched filtering are identical, as a matched filter gain of 0 is assumed. The beamforming increases the signal to reverberation ratio by 23 dB and lifts it to a level around 7 dB nearly over the whole range. The noise level surpasses the reverberation level around 20 km but in the combined signal to background ratio (B8) it only gives a minor drop of less than 1 decibel on the last 10 km.

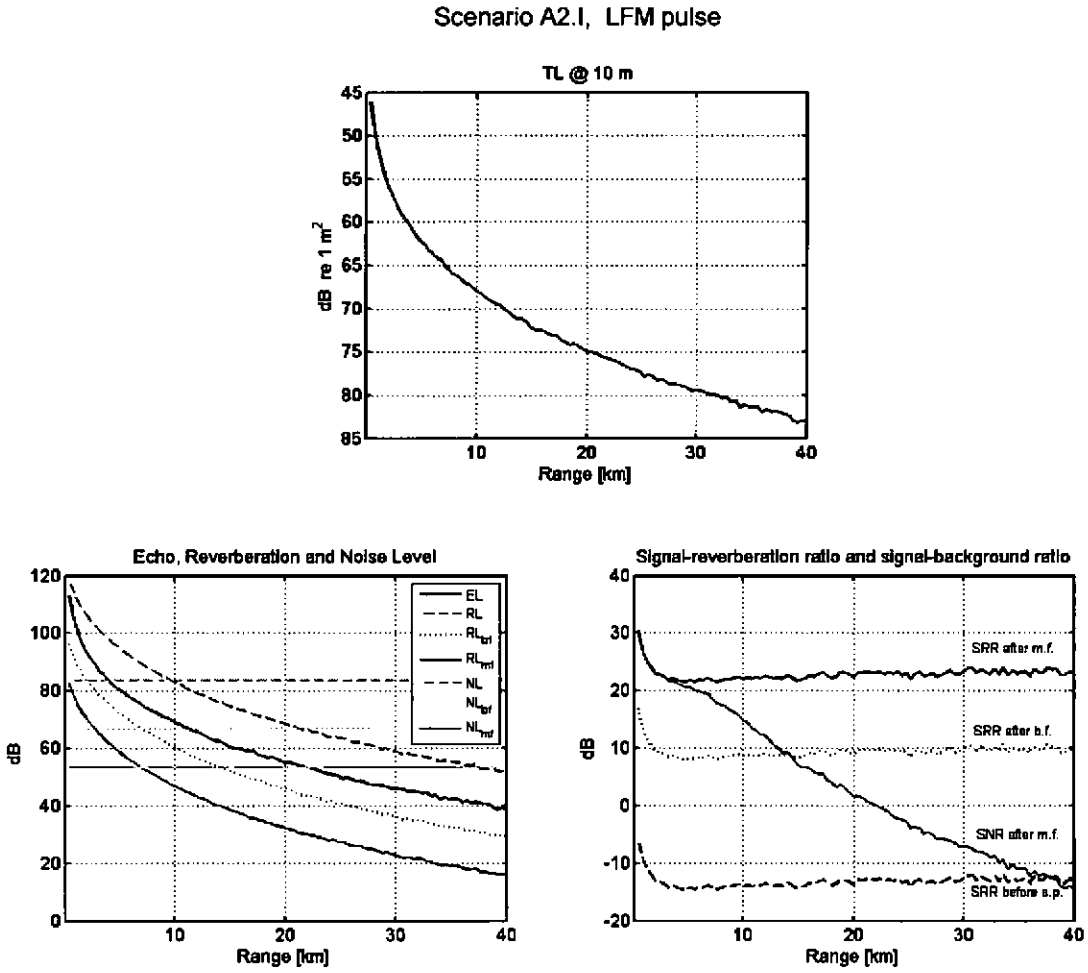


**Figure 8: Required quantities for scenario A2.I with LFM signal**

**Top:** **Transmission loss at target depth (A5),**

**Left:** **Echo level EL (A2, B1, B5) identical before and after signal processing (s.p.)**
**Reverberation level before s.p. RL (A3), after beamformer $RL_{bf}$ (B2) and matched filter $RL_{mf}$ (B6)**
**Noise level before s.p. NL (A1), after beamformer $NL_{bf}$ (B3) and matched filter $NL_{mf}$ (B7)**

**Right:** **Signal to reverberation before s.p. SRR (A4) and after beamformer $SRR_{bf}$ (B4),**
**Signal to reverberation after matched filter $SRR_{mf}$**
**Signal to background SNR (noise+reverberation) after matched filter (B8)**

Figure 8 shows the results for scenario A2.I with the LFM pulse. For this signal there is a matched filter gain of 13.5 dB both against noise and reverberation. Therefore the signal-to-reverberation values after signal processing are much higher than for the Gaussian pulse. But due to the large bandwidth the noise levels are much higher as well. In the signal-to-background ratio (SNR), where both noise and reverberation are considered, the LFM signal drops below zero around 22 km whereas the Gaussian signal stays above 6 dB over the whole range. (fig. 7).

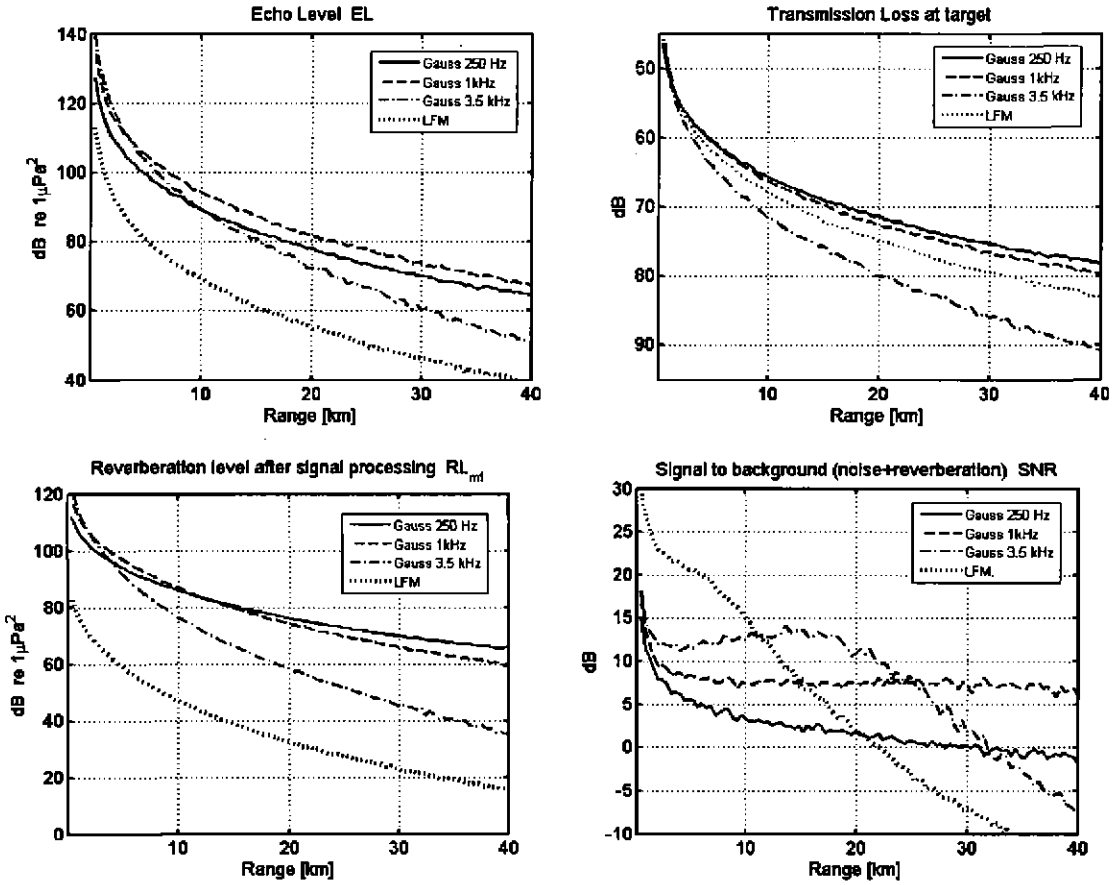


**Figure 9: Comparison between the three Gaussian pulses and the LFM pulse.**

**Top left: Echo level, top right: Transmission loss; bottom left: Reverberation level after signal processing bottom right: Signal-to-background (noise+reverberation) ratio**

Figure 9 shows a comparison between the four different signals. The transmission loss (top right) increases with frequency due to the increasing absorption. In the EL (top left) this effect is combined with the different equivalent source levels which leads to the 1 kHz signal having the highest echo level. The reverberation (bottom left) is highest for the 250 Hz signal. The LFM signal has very low reverberation due to the matched filtering. Therefore it has by far the highest signal-to-reverberation ratio. In the combined signal-to-background ratio SNR (bottom right) that includes both noise and reverberation the LFM is only good for short ranges because the increased noise level due to the large bandwidth limits the performance. The Gaussian signals are mainly reverberation limited with the 3.5 kHz signal having the highest SNR up to 25 km where again the noise deteriorates the performance.

## 5.2 Results for other problems

### 5.2.1 Scenario A2.II

Scenario A2.II differs from the basic scenario by introducing 10 m/s wind on the sea surface. Figure 10 shows the differences between the two problems for the 1 kHz Gaussian signal. The results are largely similar with slightly increased values for echo level and reverberation level for A2.II with the rough surface due to the wind. The noise level is unchanged between the two problems, but only because in the scenario definition the additional noise due to the wind was explicitly excluded. Therefore the SNR for A2.II is even higher for the wind problem compared to the basic problem.

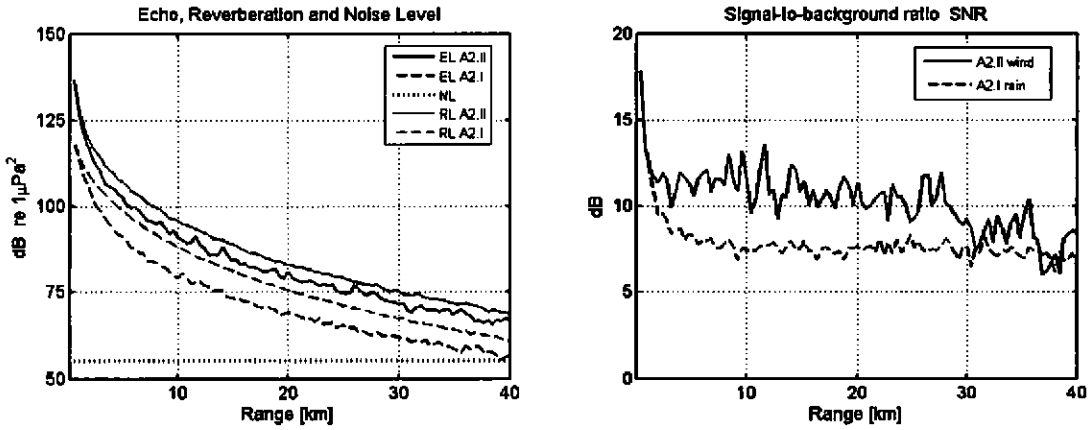


**Figure 10: Left: Comparison of echo level and reverberation level between the problems A2.II (solid lines) and A2.I (dashed lines). Right: Comparison of the signal-to-background ratios.**

### 5.2.2 Scenario A2.III, summer profile

The problem A2.III is the first with depth dependent sound speed profile. Especially the summer profile with the cut-off duct is interesting because the effect of the stochastic raytracing can be investigated. Figure 11 shows the sound velocity profile for that case.

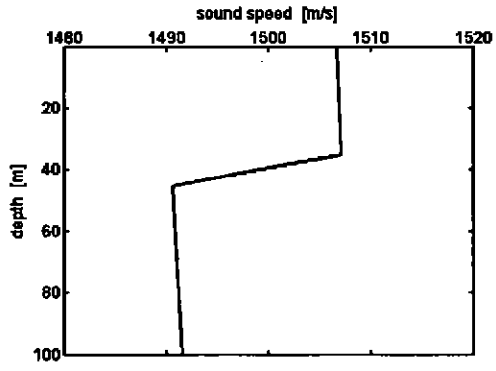


**Figure 11: Sound velocity profile for scenario A2.III summer profile**

The profile shows a weak surface duct in the mixed layer from the surface down to 35 m, the thermocline reaching to 40 m and an isothermal layer with a deeper sound channel touching the bottom at 100 m. The problem definition placed the source at 30 m depth and the receiver at 50, outside the surface duct. For the monostatic MOCASSIN calculations the receiver was moved to the position of the source (30 m), within the surface duct.

Figure 12 shows the transmission loss calculated for three different values of the parameter diffusion length $D_0$, which controls the strength of the statistic effects on the propagation. With the value of $10^{-9}$ (top left) for the calculations are practically deterministic, i.e. there are no changes in scattering angles at the cell borders The structure of the surface duct can clearly be seen. The intermediate value of $10^{-8}$ (top right) corresponds to weak statistic influence. The duct is still present but it is broadened somewhat by the scattering. With strong statistic influence ($D_0$,=$10^{-7}$, bottom left) the duct effect is almost completely washed out. This can also be observed in the plot of the transmission loss at the depth of the target (10 m) in the bottom right picture. The transmission loss increases with increasing statistic influence because more and more energy is scattered out of the duct.

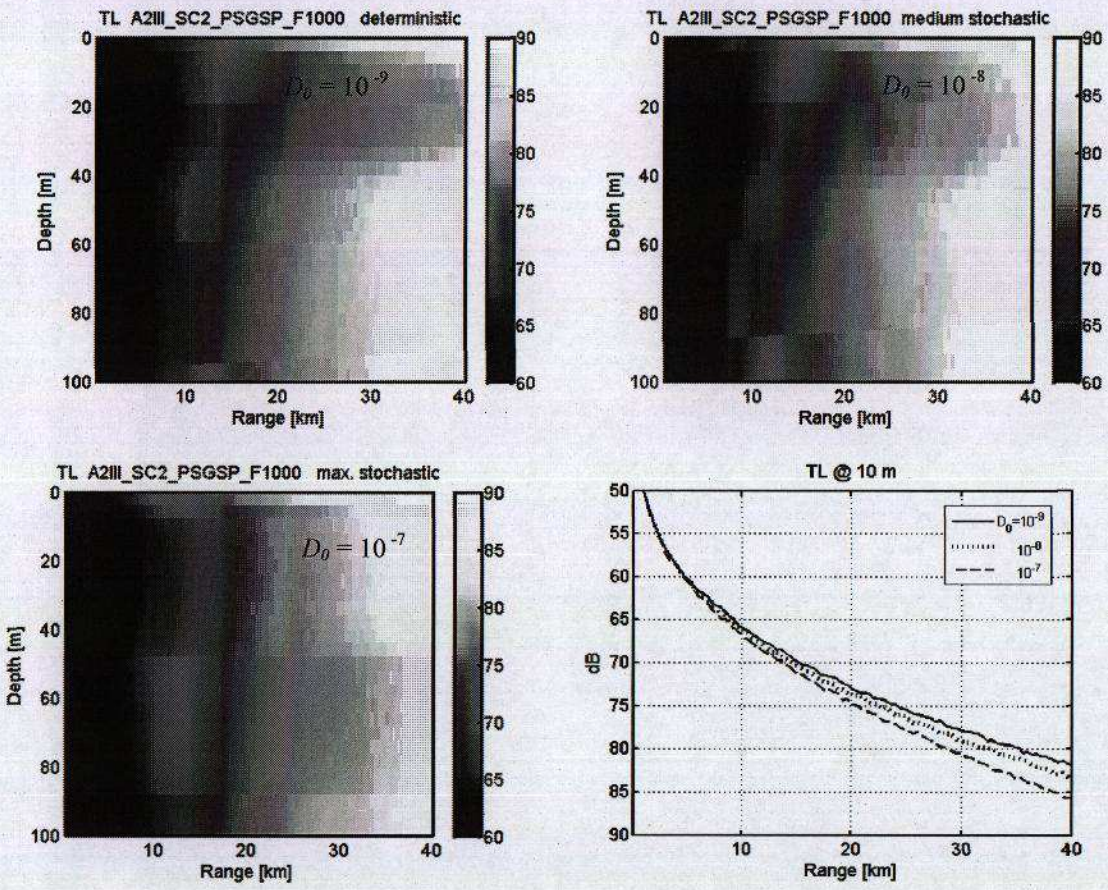


**Figure 12: Transmission loss in dB re 1 m$^2$ in the raytracing in scenario A2.III with the summer profile and the 1 kHz Gaussian signal: quasi deterministic conditions ($D_0$=$10^{-9}$), weak statistic influence ($D_0$=$10^{-8}$) and strong statistic influence ($D_0$=$10^{-7}$)**

The picture is reversed if the source is placed outside the duct. Figure 13 shows the transmission loss at 10 m depth for the source and receiver at 70 m, well below the surface duct. In this case the receiver is outside the duct and the statistic variations that cause increased scattering of energy out of the duct lead to increased energy at the receiver and hence lower transmission loss. Therefore the calculation with strong statistic influence ($D_0$=$10^{-7}$) shows the lowest transmission loss.

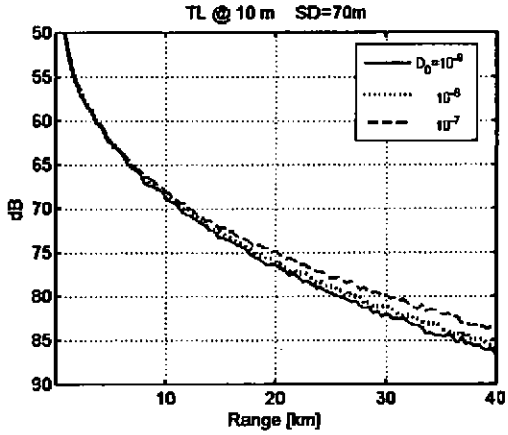


**Figure 13: Transmission loss in dB re 1 m$^2$ for quasi deterministic ($D_0=10^{-9}$), weak ($D_0=10^{-8}$) and strong statistic ($D_0=10^{-7}$) influence in the raytracing in scenario A2.III with the summer profile and the 1 kHz Gaussian signal**

# 6 SUMMARY

Calculations for the scenario A2 of the David Weston memorial symposium with the sonar performance modelling code MOCASSIN were presented. The ray tracing code MOCASSIN is the standard sonar prediction tool of the German Navy for shallow water. The basic features of MOCASSIN and the approach of statistical raytracing by a diffusion analogy were explained. Selected results of calculations for the problems A2.I, A2.II and A2.III for the different Gaussian and LFM signals were presented. In order to calculate the test problem with MOCASSIN the scenario had to be changed to a monostatic setup with source and receiver in the same place. The signal processing had to be treated by slightly simplifying assumptions. For the scenario A2.III with a non-constant sound velocity profile the effect of varying the amount of the statistic influence on transmission loss was demonstrated.

# 7 REFERENCES


1. M. Zampolli, M.A. Ainslie, "Sonar Scenario A2: LFAS vs vacuum sphere", David Weston Memorial Symposium, Proc. IOA Vol. 32, Part 2, 2010
2. W.H. Thorp, Analytic description of the low-frequency attenuation coefficient, J. Acoust. Soc. Am., Vol. 42, 270, 1967
3. APL-UW High-Frequency Ocean Environmental Acoustic Models Handbook, APL-UW TR9407, AEAS 9501, Applied Physics Laboratory, University of Washington, Seattle, 1994
4. H.G. Schneider, "Rough boundary scattering in raytracing computations", Acoustica 35, 18, 1976
5. H.G. Schneider, "Excess sound propagation loss in a stochastic environment", J. Acoust. Soc. Am., Vol. 62, 871-877, 1977
6. J. Sellschopp, Stochastic raytracing in thermoclines, In *Ocean Variability and Acoustic Propagation,* Potter and Warn-Varnas (ed.), Kluwer, 1991.
7. W. Kroll, L. Ginzkey, W. Jans, J. Pihl, J. Moren, and P. Söderberg, Measured and modeled acoustic propagation loss in the Baltic Sea, in Undersea Defence Technology Europe, Malmö, Sweden, 2003.
8. F. Gerdes, H.G. Hofmann, and I. Nissen, "Comparison of measured and modelled acoustic propagation loss in the Baltic Sea", In *Seventh European Conference on Underwater Acoustics,* D.G. Simmons, pp 51-56, 2004.
9. H.G. Hofmann, D. Brecht, F. Gerdes, "Propagation loss modelling and measurements under conditions with high spatial variability", In UDT Europe, Naples, Italy, 2007.
10. Frank Gerdes, Hans-Günter Hofmann, Wolfgang Jans, Steffen Künzel, Ivor Nissen Henry Dol, "Measurements and simulations of acoustic propagation loss in the Baltic Sea", Proc. Underwater Acoustic Measurements: Technologies & Results, Papadakis (ed.), Greece, 2009
11. R. Thiele, "A comparative test of shallow water sound propagation models against real data", SACLANTCEN Report SR 149, La Spezia, Italy, 1989
12. R.E. Francois, G.R. Garrison, Sound absorption based on ocean measurements, Parts I&II, J. Acoust. Soc. Am., Vol. 72, 896–907 & 1897–1890, 1982
13. H. Schmidt, OASES Version 2.2 User Guide and Reference Manual, Massachusetts Institute of Technology, Department of Ocean Engineering, Cambridge, 1999
14. E.L. Hamilton, Geoacoustic modelling of the sea floor, J. Acoust. Soc. Am., Vol. 68, 1313-1340, 1980
15. Schneider, Hans Georg: „Modelling wind dependent acoustic transmission loss due to bubbles in shallow water", in, "Progress in underwater acoustics",H.M. Merklinger (ed.), Plenum Press, New York, 1987
16. R.J. Christian, "The influence of a bubbly layer on near-surface acoustic propagation and surface loss modelling", NUWC Technical Document 10, New London, 1992
17. R.P. Chapman, J.H. Harris, Surface backscattering strength measured with explosive sound sources",J. Acoust. Soc. Am., Vol. 34, 1592–1597, 1962
18. R.J. Urick,"Principles of underwater sound", 3. ed., McGraw-Hill, New York, 1983
19. J. T. Kroenert, Discussion of detection threshold with reverberation limited conditions, J. Acoust. Soc. Am., Vol. 71, 507-508, 1982
20. Burdic, "Underwater Acoustics System Analysis", Prentice-Hall, Englewood Cliffs, 1984